NMR Studies of the Dynamics of Nitrophorin 2 Bound to Nitric Oxide†

Dhanasekaran Muthu[*], **Robert E. Berry**[*], **Hongjun Zhang**, and **F. Ann Walker**[*]
Department of Chemistry and Biochemistry, The University of Arizona, 1306 E. University
Boulevard, Tucson, AZ 85721-0041

Abstract

The *Rhodnius* nitrophorins are β-barrel proteins of the lipocalin fold with a heme protruding from
the open end of the barrel. They are found in the saliva of the blood-sucking insect *Rhodnius
prolixus*, which synthesizes and stores nitric oxide (NO) in the salivary glands, where NO is bound
to iron. NO is released by dilution and pH rise when the insect spits its saliva into the tissues of a
victim, to aid in obtaining a blood meal. In the adult insect there are four nitrophorins, NP1, NP2,
NP3 and NP4. At pH 7.3, NP4 releases NO 17 times faster than does NP2, as measured by
stopped-flow kinetics. A number of crystal structures of the least abundant protein, NP4, are
available. These structures have been used to propose that two loops between adjacent β-strands at
the front opening of the protein, the A-B and G-H loops, determine the rate of NO release. In order
to learn how the protein loops contribute to release of NO for each of the nitrophorins, the
dynamics of these proteins are being studied in our laboratory. In this work, the NP2-NO complex
has been investigated by NMR relaxation measurements to probe the pico- to nanosecond and
micro- to millisecond time scale motions at three pH values, 5.0, 6.5, and 7.3. It is found that at

[*]Dhanasekaran Muthu dhanas@email.arizona.edu Tel. (520-621-9697) Robert E. Berryberryr@email.arizona.edu Tel. (520-621-9697)
F. Ann Walker awalker@email.arizona.edu Tel. (520-621-8645).

Supporting Information Available. Figures showing the sequences of the four nitrophorins, the ^{1}H$\{^{15}$N$\}$ HSQC of NP2(D1A)-NO
compared to that of native N-terminus NP2-NO, the ^{15}N relaxation data and calculated modelfree order parameter (S^2) of the NP2-
NO complex measured at pH 6.5, a plot comparing the per-residue correlation time (τ_m) of the NP2-NO complex, obtained from the
R_2/R_1 ratios measured at three different pH values, the pH-dependent changes in chemical shifts for a small portion of the ^{1}H$\{^{15}$N$\}$
HSQC plot at pH 5.0 as compared to 7.3, a figure showing how the backbone ^{1}H$\{^{15}$N$\}$ HSQC anomalies are mirrored for other nuclei
of the backbone and side chains, plot of the predicted S^2 order parameters at pH 5.0 and 7.3, plot of the absolute change in φ and ψ
between pH 5.0 and 7.3, and plot of the absolute change in φ and ψ predicted at pH 7.3 and observed in the crystal structure of
NP2(D1A)-NH$_3$ at pH 7.5. Table S1 listing a summary of chemical shifts (in ppm) of NP2(D1A)-NO at pH 5.0 and 7.3, from the
assignments listed in Appendix A, Table S2, listing a summary of the *TALOS-N* output from analysis of the NP2(D1A)-NO backbone
chemical shifts, and six tables listing a summary of the relaxation data, three listing the backbone dynamic parameters from the
modelfree calculations of ^{15}N NMR relaxation data for the NP2-NO complex at pH 7.3, 6.5 and 5.0 (Tables S3, S4 and S5,
respectively) and three listing summaries of relaxation data calculated for NP2-NO complex at pH 5.0, 6.5 and 7.3 (Table S6 for ^{15}N
longitudinal relaxation rate (R_1) measurements, Table S7 for ^{15}N transverse relaxation rate (R_2) measurements, and Table S8
for ^{15}N$\{^1$H$\}$ NOE measurements), a table (S9) listing the summary of model selection with residue level details, and a table (S10)
listing a sample FASTModelfree configuration file used to run the modelfree calculations of this work. This material is available free
of charge via the internet at http://pubs.acs.org.

Appendix Information Available. Complete sequence-specific assignment tables for [^{13}C,^{15}N]-NP2(D1A)-NO obtained at pH 5.0
and 7.3; Table A1: Assignments from the ^{1}H$\{^{15}$N$\}$ HSQC experiment; Table A2: Cα-Hα assignments from the ^{1}H$\{^{13}$C$\}$ HSQC
experiment; Table A3: Cα-Hα assignments from the HBHACONH experiment; Table A4: Assignments from the HNCO experiment;
Table A5: Assignments from the HNCACB and CBCACONH experiments; Table A6: Partial Hβ assignments in the ^{1}H$\{^{13}$C$\}$ HSQC
and HBHACONH experiments (in ppm), which were used to resolve threonine Hα assignment ambiguities. This material is available
free of charge via the internet at http://pubs.acs.org.

pH 5.0 and 6.5, NP2-NO is rigid and only a few residues in the loop regions show dynamics, while at pH 7.3 somewhat more dynamics, particularly of the A-B loop, are observed. Comparison to other lipocalins shows that all are relatively rigid, and that the dynamics of lipocalins in general are much more subtle than those of mainly α-helical proteins.

Nitrophorins (NP) are ferriheme proteins which bind and carry nitric oxide and are found in the salivary glands of blood-sucking insects.[1-3] In the adult insect *Rhodnius prolixus*, which is native to the Amazon River basin, there are four such ferriheme proteins of the lipocalin fold (an 8-stranded β-barrel, with the heme inside the barrel), as shown in **Figure 1**. The structures of various ligand complexes of NP1,[4-6] NP2[7,8] and NP4[9,-,14] have been solved by X-ray crystallography. In the salivary glands, the hemes of the four proteins are bound to nitric oxide, which is synthesized by a constituitive Nitric Oxide Synthase (NOS) enzyme found in the epithelial cells of the salivary glands.[15] When the insect finds a host which can provide the blood meal it needs each month, the cherry red saliva, including its nitrophorin proteins loaded with NO, is spit into the tissues of the host at the site of the bite.[3] Dilution of the proteins and pH rise from that of the saliva (5.0-6.0) to that of the host tissues (7.3-7.4) allows dissociation of NO, which can travel through cell walls to reach nearby blood capillaries. There it can interact with the heme enzyme guanylyl cyclase to produce cyclic GMP,[16] which causes vasodilation to allow more blood to be transported to the site of the wound, thus providing the insect with a blood meal in a relatively short time period. The four nitrophorins of the adult *Rhodnius* insect each have a molecular weight of about 20 kDa, and they each have four conserved cysteine residues which form two disulfide bonds that help to maintain the 8-stranded β-barrel structures of each protein, as shown in Figure 1.[4-14] The protein sequences of the four proteins (Figure S1, Supporting Information) fall into two pairs, NP1 and NP4, which are 89% identical in sequence, and NP2 and NP3, which are 79% identical. The abundances of NP1-NP4 in the insect saliva are 49, 21, 20 and 10%, respectively.[3] The two pairs of NPs have very different NO release rates, with NP4 and NP1 releasing NO 17 and 12 times faster than NP2 at pH 7.5 (k_{off} = 1.6 s^{-1} and 1.1 s^{-1}, respectively (Berry, R. E., unpublished results) vs. 0.093 s^{-1},[17] respectively, both at 27 °C and pH 7.5). Understanding the dynamics of loop motions is very important for developing a full understanding of the behavior of the *Rhodnius* nitrophorins.

Also important to the dynamics of loop motions is that the recombinantly-produced proteins have the same N-termini as do the native proteins. As shown in Supporting Information Figure S1, three of the four proteins, NP1, NP2, NP3 have a charged amino acid as the first amino acid of their mature proteins. These three NPs, when expressed in *E. coli*, retain the Met0 that arises from translation of the start codon. In contrast, NP4, whose first amino acid is Ala, does not have Met0 when isolated and purified. This is thought to be a result of the fact that the *E. coli* methionine aminopeptidase is able to cleave Met0 from proteins whose first amino acid has a small hydrophobic side chain, but cannot cleave it from proteins whose first amino acid has a larger, charged side chain. In order to remove Met0 from NP1, NP2 or NP3 it is necessary to express the genes in a plasmid (pET-26b (Novagen)) that contains an export sequence before the start of the gene. This export sequence is cleaved when the protein reaches the periplasm. The cleavage produces a protein which has its native N-terminal amino acid as the first amino acid, which is able to fold properly, and form the correct disulfide bonds. Because heme synthesis is turned on by the properly-folded apoprotein, heme is synthesized and inserted into the folded protein to produce the holoprotein.

As another means of removing Met0 from NP1, 2 and 3, it was reasoned that creation of the D1A mutant of the NP2 or NP3 gene, or the K1A mutant of the NP1 gene, should give a protein having no Met0. This was found to be the case for NP2(D1A),[18] as well as

NP3(D1A) and NP1(K1A) (unpublished work). NP2(D1A) is usually expressed under conditions that produce inclusion bodies.[18] When these inclusion bodies are renatured and purified, followed by hemin addition, a stable holoprotein is produced which has no Met0, but rather, as first amino acid, has Ala rather than Asp. More recently we have shown that NP2(D1A) and native N-terminus NP2 have NMR spectra which are essentially identical.[17] Both native N-terminus NP2 and NP2(D1A) have been used in the dynamics studies reported in this work.

Montfort and coworkers have investigated the kinetics of NO release from NP4 by stopped-flow kinetics,[19] by cryocrystallography and infrared spectroscopy of NO and CO binding to NP4,[20] by femtosecond coherence spectroscopy (FCS) in combination with polarized resonance Raman spectroscopy and density functional theory (DFT) studies of NO binding to NP4,[21] by ultrafast kinetics of NO release from NP4,[22] and by 2-dimensional Fourier transform infrared spectroscopy[23] to try to understand the mechanism of NO release. Knipp et al. have investigated the infrared and resonance Raman spectra of the Fe^{II}-CO complex and have studied association and dissociation of CO to/from Fe(II) NP4 and NP7 by nanosecond laser flash photolysis and stopped flow kinetics.[24] In both cases of infrared investigations,[23,24] two vibrational frequencies were detected, one ascribed to the "closed" and the other to the "open loop" structure. Montfort et al. have found that the off-rate of NO from NP4 is proportional to the open loop state population, as well as to the pH-dependent kinetic amplitude of escape from the open pocket.[22] When both factors are considered, the off-rate increases by more than an order of magnitude when the pH is changed from 5 to 8.[22] The fast phase of NO rebinding is assigned to a conformation of the ferric protein with a closed hydrophobic pocket, while the slow phase is assigned to the protein in an open conformation with a more hydrophilic heme pocket environment.[22,23] The relative amplitude of the slower phase increases dramatically as the pH is raised from 5 to 8.[22]

With regard to the 2D FTIR studies of NP4-NO,[23] we have shown that this ligand complex of NP4 is a dimer at the two pH values used, 5.1 for the closed loop studies, and pH 7.9 for the open loop studies. The concentration of the pH 5.1 sample used in these studies was 6.4 mM and that of the pH 7.9 sample was 4.1 mM.[23] We have investigated NP4-NO by NMR spectroscopy at pH 7.3, from 3.7 mM to 0.88 mM, and found very broad $^1H\{^{15}N\}$ HSQC spectra that are consistent with *either* a mixture of NP4-NO monomer and dimer, *and/or* NP4-NO dimer in exchange with the monomer on the NMR timescale (Berry, R. E, unpublished results). Considering the sizes of the broad peaks, rates in the range of ~150 s^{-1} are suggested. At pH 5.0, 0.2 mM, NP4-NO is a dimer with a well-resolved $^1H\{^{15}N\}$ HSQC spectrum which can be investigated by NMR techniques (Berry, R. E., unpublished results). Thus, it will be necessary to re-think what the results of the 2D FTIR studies[23] mean, since not only are the measurements made on the dimeric form of NP4, but the structures used to explain the data are all those of monomeric NP4-NO, crystallized in the presence of high salt and/or PEG.[9-14] The side chains shown to be important in dimer formation are D30, others in the A-B loop and D132, as well as the heme carboxylates (Berry, R. E., unpublished results).

In comparison to NP4, the rate of NO release from native N-terminus NP2 changes by only a factor of three between pH 5 and 7.5,[17] suggesting that although all four nitrophorins have D29(30), not all are similarly affected by pH change, and that there is thus a need to investigate all four proteins by the same techniques in order to determine the factors that affect the rates of NO release of each. In addition, NP2 shows no tendency to aggregate or form a dimer as a function of concentration and/or pH. It is striking that the major difference between the A-B and G-H loops of NP2 and NP4 is that NP2 has one less amino acid in the A-B loop (Supporting Information Figure S1), and that this could cause such dramatic differences between the behavior of NP2 and NP4 (if this is the factor which determines NO

dissociation rates). A further difference is that NP4 (and NP1) both have two prolines in the A-B loop, while NP2 and NP3 each have only one, Supporting Information Figure S1. All four NPs have an aspartic acid as the first residue of the A-B loop, and for NP4, Asp30 is believed to be the major factor which determines whether the A-B loop is open or closed.[19] Most crystal structures of NP4 obtained at pH 5.6 show a hydrogen-bond between D30 side chain carboxyl and L130 carbonyl.[10,11] Although all crystal structures of NP4-NO have the closed loop structure at all pH values, at pH 7.5 for other ligand complexes of NP4 this hydrogen-bond is not present, D30 and L130 are much farther apart, and the A-B and G-H loops are "open." [9] No NP2 crystal structure determined at pH 6.5 shows a hydrogen-bond between these two residues, D29 and L129,[7,8] and no lower-pH structures are available. The typical distance between D29 and L129 in the pH 6.5 structures is 4.96 Å.[7,8]

In an attempt to understand how the A-B and G-H loops could create such different NO release rates, we have undertaken an investigation of the loop dynamics of the NPs, beginning with the NO complex of native N-terminus NP2, [17] which is diamagnetic. Our reason for beginning with NP2 is that unlike the other three NPs of the adult insect, NP2 has a large preponderance of one of the two possible heme orientations (1:12) which result from the unsymmetrical nature of protohemin, shown in Supplementary Information Figure S2. Thus for NP2, there is only one observed ^{1}H{^{15}N} HSQC crosspeak for each backbone amide proton. In comparison, for NP4, to which we wish to compare the results of this work, the **A:B** heme orientation ratio is ~1:1, and thus there are two NH crosspeaks for each peptide NH, which may be close enough together to make it difficult to choose one or the other for dynamics investigations, or to treat both at the same time. Therefore, it is necessary to reconstitute the NP4 apoprotein with the so-called "symmetrical hemin," 2,4-dimethyldeuterohemin, in which the two vinyl groups have been replaced with methyls. This produces a heme with two less carbons than protoheme, which could potentially change the dynamics of the protein by removing some steric interactions that may be responsible for ruffling of the heme.[25]

The original report of the Lipari and Szabo modelfree analysis method for extracting parameters related to the fast timescale motions in the range of picoseconds (ps) to nanoseconds (ns) from experimental relaxation parameters was published in 1982,[26,27] and has undergone some modifications since.[28-31] The Carr-Purcell-Meiboom-Gill (CPMG) experiment for investigating microsecond to millisecond timescale dynamics and related methods were published and modified more recently.[32-39] Since those times, backbone dynamics of probably hundreds of proteins have been reported in the literature, of which we cite only a few.[35-43] We have investigated the pico- to nanosecond and the micro- to millisecond dynamics of native N-terminus NP2 by well-known methodologies. In these studies we have found that the NP2-NO complex is a fairly rigid protein, which nonetheless shows dynamics in some residues, particularly those located in the loops, and an increase in dynamics on all timescales as the pH is raised from 5.0 to 6.5 to 7.3.

Materials and Methods

Expression and purification of protein

Except where indicated, materials were obtained from Sigma-Aldrich and used without further purification. A successful method for producing native N-terminus NP2 protein has been developed in our laboratory. The detailed description of protein expression and purification has been published recently,[17] and a modified version was employed to express and purify a ^{15}N enriched sample. An overnight culture of *ArcticExpress*-(DE3) *E. coli* cells (Stratagene) containing the NP2 expression plasmid in pET-26b (Novagen) was prepared and used to inoculate (20 mL per liter) LB broth containing 100 μg/mL (172 μM) kanamycin sulfate (IBI Scientific). This was grown at 30 °C in a shaker-incubator (235 rpm)

until an OD_{600nm} of 0.8 was reached (3 hours), before being cooled to ~12 °C. The cells were collected by gentle centrifugation (1,400g for ~3 minutes) and, to maximize the final yield,[44] the cells from 2 L of growth were resuspended in 1 L of a defined minimal medium[45] (TEKnova, Hollister, CA, USA) containing 50 mM sodium chloride, 40 mM 3-morpholinopropane-1-sulfonic acid (MOPS), 11.1 mM D-glucose, 4 mM tricine, 1.32 mM dipotassium phosphate, 0.52 mM magnesium chloride, 0.28 mM potassium sulfate, 0.01 mM iron(II) sulfate, 0.5 μM calcium chloride, 0.4 μM boric acid, 80 nM manganese dichloride, 30 nM cobalt dichloride, 10 nM copper(II) sulfate, 10 nM zinc sulfate, 3 nM ammonium molybdate, and 18.7 mM ^{15}N ammonium chloride (99% isotopic enrichment, from Cambridge Isotope Laboratories, Inc.) as the sole significant bio-available source of nitrogen. This was grown at 12.5 °C in a shaker incubator (235 rpm). After 1 hour expression was induced with 1 mM isopropyl β-D-1-thiogalactopyrano-side, and the medium was supplemented with 0.1 mM 5-aminolevulinic acid, 40 μM iron(II) sulfate, and 10 μM each of thiamine HCl, pantothenic acid, 4-hydroxybenzoic acid , 4-amino-benzoic acid , and 2,3-dihydroxybenzoic acid. Additional supplements of 0.1 mM 5-amino-levulinic acid and 40 μM iron(II) sulfate were added after 2 and again after 4 days of growth. After 6 days the cells were harvested by centrifugation. The [U-^{15}N]-NP2 protein was then isolated and purified as described previously.[17] The final yield of purified protein was about 1 mg per L of minimal medium growth (as compared to ~3 mg/L using unlabeled LB). Care was taken to be certain that the heme orientation had reached equilibrium (**A:B** = 1:12 at pH 7.0)[17] by checking the NMR spectra of the high-spin hemin resonances over a period of at least 8 days before the samples were used for multidimensional NMR investigations.

Triple resonance experiments required for the assignment of the protein backbone need large amounts of ^{13}C and ^{15}N isotopically enriched protein. The soluble expression method described above yields sufficient ^{15}N enriched protein necessary for most of the dynamics experiments performed in this work, but the yield is too low for the economically-viable production of a $^{13}C,^{15}N$ doubly isotopically enriched sample. In addition, to avoid any dilution of the ^{13}C isotope, the initial unlabeled LB growth prior to re-suspension in labeled medium needed to be avoided, resulting in a yield much less than 1 mg/L. A previously described method used to produce $^{13}C_6,^{15}N_3$-histidine-enriched NP2 protein yielded ~4 mg/ L,[46] but required isotopically enriched amino acids, both the doubly labeled histidine and the non-labeled other nineteen amino acids.[46]

Thus, a much higher-yielding (~10 times) inclusion body method was used, and employed the NP2(D1A) construct[18] which is 'native-like' with respect to NMR spectroscopy, having $^1H\{^{15}N\}$ HSQC chemical shifts for its NO adduct that are within an average of ±0.005 ppm (calculated from chemical shift data shown herein) of those of the ^{15}N-labeled native N-terminus NP2-NO (hereafter called simply NP2-NO).[17] A defined minimal medium was prepared as described above (with 100 μg/mL (172 μM) kanamycin sulfate and supplemented with 10 μM each of thiamine HCl, pantothenic acid, 4-hydroxybenzoic acid, 4-aminobenzoic acid, and 2,3-dihydroxy-benzoic acid) and included, as the sole significant bio-available source of nitrogen and carbon, 18.7 mM ^{15}N ammonium chloride and 11.1 mM ^{13}C D-glucose (99% isotopic enrichment, from Cambridge Isotope Laboratories, Inc.). Part of this $^{13}C,^{15}N$ minimal medium was used to prepare an overnight culture of BL21(DE3) *E. coli* cells (Stratagene) containing the NP2(D1A) expression plasmid,[18] in pET-24a (Novagen), and was used to inoculate (20 mL per liter) the rest of the $^{13}C,^{15}N$ minimal medium. This was grown at 37 °C in a shaker-incubator (235 rpm) until an OD_{600nm} of 0.8 was reached (~3 hours). The temperature was then set to 25 °C, and after 20 minutes, expression was induced with 1 mM isopropyl β-D-1-thiogalactopyranoside. The cells were harvested by centrifugation the next day. The [U-$^{13}C,^{15}N$]-NP2(D1A) insoluble inclusion bodies were then isolated as described previously,[47] except that sonication was used to lyse the cells (50% duty cycle for 2 minutes, then 1 minute cool down, repeated 5

times) and all Tris-based buffers were substituted with 100 mM sodium phosphate buffers at pH 7.5. The isolated insoluble inclusion bodies were refolded using an improved folding method based on one described previously.[48]

The isolated inclusion bodies (less than 5 g) were dissolved in 120 mL denaturation buffer (10 mM MOPS, pH 7, 6 M guanidine HCl (Thermo Scientific), 1 mM EDTA (VWR International), 2 mM tris(2-carboxyethyl)phosphine HCl (EMD Biosciences), 1 mM dithiothreitol), stirred at room temperature for 3 hours, then rapidly diluted into 1.2 L refolding buffer (10 mM MOPS, 1mM L-glutathione reduced, 0.29 M sucrose, 0.5 M L-arginine, adjusted to pH 7.0), and stirred overnight at 4 °C. The refolded protein was then dialyzed (Spectra/Por® membrane tubing 14,000 MWCO) twice against dialysis buffer (10 mM MOPS, 0.29 M sucrose, 50 mM L-glutamic acid, 50 mM NaCl, adjusted to pH 7.0). The now natively-folded, soluble *apo*-protein was concentrated to about 50 mL and titrated with a large excess of hemin (5 mL of ~2 mM hemin dissolved in a few drops of 1 M KOH and diluted into pH 7.5 100 mM sodium phosphate buffer) to form the *holo*-protein. The pH was reduced to pH 5.5 with acetic acid and the excess hemin precipitate was then removed by high speed centrifugation. The sample was further concentrated to ~5 mL before being loaded onto a gel filtration column (a 5 mL pre-packed HiTrap desalting guard column connected in series with a HiPrep 26/60 Sephacryl S-100 HR column, GE Healthcare, equilibrated with 100 mM sodium acetate buffer at pH 5 with 100 mM NaCl). The peak fraction eluted from the gel chromatography was dialyzed against 30 mM sodium acetate buffer at pH 5 before being further purified by cation exchange chromatography. In no more than 5-mg batches, the dialyzed nitrophorin was loaded onto a cation exchange column (two 5 mL HiTrap SP HP columns connected in series), washed with 20 mL of the 30 mM sodium acetate buffer at pH 5 and eluted with a salt gradient (1 M NaCl in 30 mM sodium acetate buffer). Pure [U-^{13}C,^{15}N]-NP2(D1A) eluted as a single peak at an ionic strength of ~4 mS/cm. The final yield of [U-^{13}C,^{15}N]-NP2(D1A) was about 10 mg per L of minimal medium growth. Care was taken to be certain that the heme orientation had reached equilibrium (**A:B** = 1:14 at pH 7.0)[18] by checking the NMR spectra of the high-spin hemin resonances over a period of at least 8 days before the samples were used for multidimensional NMR investigations.

Preparation of NMR samples

Stocks of NMR buffers were prepared at pH 5.0 (50 mM sodium acetate with 95% H$_2$O and 5% D$_2$O), pH 6.5 and pH 7.3 (both 50 mM sodium phosphate with 95% H$_2$O and 5% D$_2$O). The purified [U-^{15}N]-NP2 and [U-^{13}C,^{15}N]-NP2(D1A) proteins were exchanged four times into the appropriate NMR buffer (using Centriprep 10,000 MWCO centrifuge concentrators), and immediately before the samples were loaded into Shigemi NMR tubes, a few crystals of S-nitroso-N-acetyl-D,L-penicillamine were added as a source of nitric oxide;[49] this compound releases NO with a half-life of less than 30 s. Escape of the nitric oxide was inhibited by the tight seal of the Shigemi tubes' matched plunger, and the nitric oxide complex was found to be stable for months (confirmed by ^{1}H{^{15}N} HSQC). And since the heme does not leave the protein once NO or other ligand is added, the NO complex could be maintained at the **A:B** ratio of 1:14 for NP2(D1A) or 1:12 for native N-terminus NP2, even at pH 5.0. Sodium 3-(trimethylsilyl)-1-propanesulfonate (DSS, from Cambridge Isotope Laboratories, Inc.) was added to the samples for chemical shift reference. The concentration of the [U-^{15}N]-NP2-NO and [U-^{13}C,^{15}N]-NP2(D1A)-NO samples were about 0.2 and 2 mM, respectively. It should be noted that because both NO and iron(III) are odd-electron systems, the NO complex of NP2 is diamagnetic.

Sequence-specific assignments of [^{13}C,^{15}N]-NP2(D1A)-NO and relaxation data for [^{15}N]-NP2-NO

2D ^{1}H{^{15}N} HSQC spectra were initially used to identify the number of spin systems and confirm that no high-spin NP2(D1A)-H$_2$O remains (additional nitric oxide was added if needed to completely complex all of the NP2(D1A), recorded locally on a Varian Inova 600 equipped with a cryogenic probe). The presence of excess NO(g) does not interfere in any way with the NMR experiments, based on the chemical shifts and ^{15}N T_1s of NP2-NO recorded with excess NO and with a sample extensively washed (repeatedly diluted and re-concentrated) to remove any excess NO (at pH 5.0). The rest of the 2D and 3D heteronuclear NMR spectra for the sequence-specific assignments of [U-^{13}C,^{15}N]-NP2(D1A)-NO were recorded at the National Magnetic Resonance Facility at Madison (NMRFAM) on a 600 MHz Bruker AVIII-600i equipped with a 5 mm TXI cryoprobe, and relaxation data for [U-^{15}N]-NP2-NO were collected on a 600 MHz Varian NMR spectrometer equipped with a cryogenic probe. The temperature was maintained at 30 °C. 2D ^{1}H{^{15}N} HSQC, 3D HNCO, 3D HNCACB and 3D CBCA(CO)NH peak lists were used as input to the PINE server,[50] and employing the PINE-SPARKY extension,[51] were used to determine sequence-specific backbone resonance assignments. 2D ^{1}H{^{13}C} HSQC and 3D HBHA(CO)NH experiments were used to assign the ^{1}H$^\alpha$ resonances. Assignment data were collected at pH 5.0 and 7.3, referenced to DSS,[52] and are listed in the Supporting Information, **Table S1**. This is a summary of all the backbone chemical shifts assigned, and represents an average of all of the assignments of the experiments listed in **Appendix A**. The carbonyl chemical shifts were obtained from the assignments in the HNCO experiment (**Table A4**). The Cα and Cβ chemical shifts are the average chemical shifts obtained from the assignments of the ^{1}H{^{13}C} HSQC, HNCACB and CBCACONH experiments (**Tables A2 and A5**). The Hα chemical shifts are the average chemical shifts obtained from the assignments of the ^{1}H{^{13}C} HSQC and HBHACONH experiments (**Tables A2 and A3**). The amide ^{1}H shifts are the average chemical shifts obtained from the assignments of the ^{1}H{^{15}N} HSQC, HNCO, HNCACB, CBCACONH, and HBHACONH experiments (**Tables A1 and A3-5**). The amide ^{15}N shifts were obtained from the assignments of the ^{1}H{^{15}N} HSQC experiment (**Table A1**). These chemical shifts were used to obtain backbone torsional angles using *TALOS* (Torsion Angle Likelihood Obtained from Shift and sequence similarity),[53-55] specifically the version *TALOS-N*,[55] (which also derives side-chain χ_1 angle information), and reports an estimated backbone order parameter S^2 derived from the chemical shifts.[56]

All data were processed with the *NMRPipe*[57,58] suite and visualized with *SPARKY*.[59] All relaxation data for [U-^{15}N]-NP2-NO are listed in the Supporting Information, Tables S3 – S8.

^{15}N Relaxation and Modelfree calculations

^{15}N longitudinal (T_1) and transverse (T_2) relaxation experiments were performed at 30 °C on a Varian 600 MHz spectrometer in an interleaved manner with a few duplicate points for error estimation. T_1 and T_2 experiments were collected with 64 scans, 1024×200 complex data points. A recycle delay of 1.5 seconds was used between the scans. For T_1 measurements a total of 13 spectra were recorded using T_1 delays of 0.01, 0.02 (x2), 0.06, 0.12 (x2), 0.22, 0.42 (x2), 0.64, 0.96 (x2) and 1.28 seconds. For T_2 measurements a total of 14 spectra were recorded using T_2 delays of 0.01, 0.03 (x2), 0.05, 0.07 (x2), 0.09, 0.11 (x2), 0.13, 0.15 (x2), 0.17 and 0.19 seconds (duplicates are indicated by the x2). The ^{15}N{^{1}H} *NOE* experiments were acquired with 256 scans in a 1024×120 data matrix with a recycle delay of 4.5 seconds in an interleaved fashion. The relaxation data T_1, T_2 and ^{15}N{^{1}H} *NOE* were analyzed using *SPARKY*.[59] The intensities of the amide resonances were obtained by measuring the heights of the peaks in the spectra, a routine available within the *SPARKY*

program. Uncertainty measurements were made from duplicate spectra acquired independently.

The relaxation rates R_1 and R_2 were obtained by exponential curve fitting of relaxation times T_1 and T_2 using the program *RELAX*.[60] The *RELAX* program was also used to calculate the $^{15}N\{^1H\}$ heteronuclear steady-state NOEs from the I_{sat}/I_{unsat} ratios, where I_{sat} and I_{unsat} are the peak intensities in the spectra collected with and without proton saturation, respectively. Uncertainty measurements for modelfree calculations were obtained using the RELAX program either from duplicate spectra acquired independently or from spectral noise using the baseplane error estimation routine available within the program. The estimated errors are in the 2-4% range for R_1 and R_2, and 4-8% range for the NOE, with few exceptions. An initial guess of the molecular rotational diffusion tensor and overall correlation time (τ_m) was obtained from the R_2/R_1 ratio of the individual ^{15}N amide peaks using the programs 'r2r1_tm' and 'quadric_diffusion' developed by the Palmer group,[61] which follows the approach of Brüschweiler et al.[62] and Lee et al.[63] The X-ray structure of NP2(D1A)-NH$_3$ (PDB code 2EU7), was used for this purpose and for subsequent modelfree calculations. The PDB file for modelfree calculation was prepared by adding hydrogen atoms using the program UCSF-Chimera[64] followed by translation to the center of mass with program 'pdbinertia' developed by the Palmer group. The final PDB file was used as an input for the modelfree calculations. The *FASTModelfree* program developed by Cole and Loria[30] was used to accomplish the modelfree calculations. The *FASTModelfree* program interfaces with the program Modelfree 4.1 developed by the Palmer group to perform the rigorous statistical testing protocols for the assignment of model functions for each individual residue. Moreover, it requires minimal user involvement in preparing the input files. The ^{15}N chemical shift anisotropy (CSA) and the distance N-H bond length (r_{N-H}) used in the calculations were −172 ppm and 1.02 Å respectively, which seem good choices as they have been used in most of the recent protein dynamics studies.[40] The *FASTModelfree* configuration file, showing all the parameters used in the calculations, is provided as Supplementary Information Table S10. The results from 'quadric diffusion' calculations, especially the $D_\parallel/D_\perp$ ratio, suggested an axially symmetric diffusion tensor for the modelfree calculations. Thus, out of two available choices (isotropic or axially symmetric) for the diffusion tensor in the *FastModelfree* program, an axially symmetric diffusion tensor was chosen for all calculations.

Relaxation dispersion analysis

All of the ^{15}N R_2 relaxation experiments were recorded on a Varian 600 MHz spectrometer at 30 °C using the relaxation-compensated CPMG pulse sequence described previously by Kay et al.[32] The constant time delay was set to 0.06 seconds. A series of 22 spectra were recorded with CPMG, ν_{cp}, of 66.7, 133.3, 200 (x2), 266.7, 333.3, 400 (x2), 466.7, 533.3, 600 (x2), 666.7, 733.3, 800 (x2), 866.7, 933.3, 1000 (x2) Hz (duplicates are indicated by the x2). In addition, a reference spectrum without any CMPG component in the pulse sequence was also recorded in duplicate. Each 2D spectrum was acquired as a complex data matrix of 512×256 with 32 scans per FID and 2.2 seconds delay between scans. *SPARKY*[59] was used to analyze the data to obtain the peak heights for curve fitting to get the effective transverse relaxation rates (R_2^{eff}). The program *NESSY*[65] was used for the curve fitting. The *SPARKY* peak height list files were directly used in the *NESSY* program. Since all ^{15}N relaxation data showed flat relaxation plots, R_2 vs delay (no observed decay curves), $\Delta R_2^{eff}(\nu_{CPMG})$ two-point values were calculated using the following equation:

$$\Delta R_2^{eff}(\nu_{CPMG}) = \frac{1}{Tcp}\ln\left(\frac{I1000}{I66.7}\right) \quad (1)$$

where I_{1000} and $I_{66.7}$ are the heights of cross-peaks in spectra collected at effective CPMG fields of 1000 and 66.7 Hz, respectively, and T_{cp} is the constant time delay (0.06 seconds).

Results

Backbone sequential assignment of the NP2-NO complex, and analysis of the chemical shift differences between pH 5.0 and 7.3

It is necessary to have the ^{15}NH assignments in order to interpret the relaxation data. The mutant NP2(D1A) was used to obtain the backbone sequential assignments, because it is easier to produce uniformly labeled (^{13}C and ^{15}N) protein in larger quantity than is possible for the native N-terminus NP2 protein itself (hereafter simply called NP2). It has been shown previously that NP2(D1A) and native N-terminus NP2 have essentially identical chemical shifts of all resonances,[17] and we show in this work that the ^{1}H{^{15}N} HSQC spectra have almost identical chemical shifts for the vast majority of the resonances for the two nuclei of these two proteins, as shown in Supporting Information Figure S3. The HNCACB and CBCACONH experiments were recorded on uniformly ^{13}C- and ^{15}N-enriched NP2(D1A)-NO samples to effect the sequential assignments. Assignments were made at two pH values, 5.0 and 7.3, because it was found that the ^{1}H,^{15}N chemical shifts were significantly different at these two pH conditions, as shown in **Figure 2a**. The chemical shift assignments of NP2(D1A)-NO at pH 5.0 were used to assign the HSQC spectrum of native N-terminus NP2-NO at pH 6.5 because of the similarity in chemical shift values at pH 5.0 and 6.5, as shown in Figure 2b. The ^{1}H and ^{15}N chemical shifts of NP2(D1A)-NO at pH 5.0 and 7.3 are presented in the Supporting Information, Table S1. Complete assignment data are presented in the six tables of Appendix 1.

The observed chemical shift values of backbone protons and nitrogens are relatively similar at both pH 5.0 and 7.3 for all residues except those located in the A-B and G-H loops, as seen in **Figure 3** for native N-terminus NP2-NO, in some cases up to a 2 ppm change in ^{15}N chemical shifts occurs over this pH range, and in some cases over 0.5 ppm change in proton chemical shifts. The same is observed for NP2(D1A)-NO, as seen in Supporting Information Figure S3, and this chemical shift pH dependence extends to all the atoms of NP2(D1A)-NO assigned in Table S1, as can be seen in Supporting Information Figure S4. These observations encouraged us to examine the possibility of structural changes resulting from pH changes using the well-established *TALOS+* (Torsion Angle Likeliness Obtained from Shift and Sequence Similarity)[54] program using the chemical shifts of NP2(D1A)-NO. The *TALOS-N*[55] program is an improved version of the very commonly used *TALOS+* software,[53] for empirical prediction of protein backbone dihedral angles (ϕ and ψ) to within $\pm 13°$ of the crystal structure values from experimentally determined chemical shift values. *TALOS-N* also derives side-chain χ_1 angle information, and reports an estimated backbone order parameter S^2 derived from the chemical shifts.[56] A summary of the output from the *TALOS-N*[55] program is listed in Supporting Information Table S2.

The predicted order parameters (S^2) show reduced values associated with protein loop regions, and increased dynamics at pH 7.3 relative to pH 5.0, most notably at the A-B loop, E-F loop, and G-H loop regions near the opening to the heme pocket (see Supporting Information Figure S5). The predicted ϕ and ψ angles are very similar at both pH values (mostly within less than 10°), with the exception of some of the residues in the A-B and G-H loops (see Supporting Information Figure S6; notably K127 ψ and D128 ϕ angles of the G-H loop change significantly with pH), suggesting that the structure of the loop regions is somewhat changed between low and higher pH values. This observation, combined with increased R_2 values (described in the next section), suggest that dynamics, and not structural changes, could be the reason for the chemical shift differences between the two pH values. *TALOS-N* analysis also revealed that the conformations of the A-B and G-H loops are

different in solution from those seen in the crystal structure of NP2(D1A)-NH$_3$ at pH 7.5 (PDB file 2EU7), but this is not true for other parts of the protein (Supporting Information Table S2). The 3-state χ_1 side-chain torsional angles, where they have been predicted, do not change over this pH range (Supporting Information Table S2). Some predicted values are significantly different at pH 5.0 from those at 7.3, as indicated in Supporting Information Figure S7, suggesting that there are major changes in loop conformations as a function of pH. However, the differences in predicted structure at pH 7.3 in solution with NO bound and the observed crystal structure at pH 7.5 with NH$_3$ bound (PDB file 2EU7)[8] are relatively small, except for a few residues in the A-B and GH loops, as shown in Supporting Information Figure S8. At this pH the loops should be open. Thus one would not expect major conformational differences as a function of ligand. Notable changes as compared to the crystal structure are: A type I β-turn is predicted at D31 to V34 that is not observed in the NP2(D1A)-NH$_3$ crystal structure obtained at pH 7.5. Similarly, type II' β-turn dihedral angles are predicted for the segment E124-G125-S126-K127, but a type IV β-turn is seen in the NP2(D1A)-NH$_3$ crystal structure.[8] Nevertheless, loop changes seen for NP2 by NMR chemical shifts as a function of pH are certainly not as extreme as those seen for NP4 on the basis of X-ray crystallography.[9-14] This is one of the reasons that we began our study of the dynamics of the nitrophorins with NP2, because we suspected that such major changes would not be seen as a function of pH. In fact, this is one of the findings of the picosecond molecular dynamics simulations for NP2-NO discussed below, that the large changes in loop conformation seen for NP4-NO are not observed for NP2-NO.

Interestingly, NP4 structures obtained at low pH[‡] show a 3$_{10}$ helix for the three residues P33-D34-D35. NP4 also has a second proline in its A-B loop, P37, but that proline is not involved in a helix. No structures of NP2 have been obtained below pH 6.5, and we have been unable to grow crystals of NP2 at pH values of 5.0-6.0. Changes in the ^{1}H,^{15}N backbone chemical shifts of almost all other residues of NP2(D1A)-NO (or NP2-NO) at pH 7.3 as compared to 5.0, were insignificant.

Fast timescale dynamics

It is well documented in the literature that the fast timescale motions (picoseconds to nanoseconds) of proteins can be derived from a suite of relaxation experiments: ^{15}N longitudinal relaxation rate (R_1), transverse relaxation rate (R_2) and steady-state ^{15}N{^{1}H} NOE.[26,27,66,67] For native N-terminus NP2-NO these measurements were carried out at three different pH values, 5.0, 6.5 and 7.3.

The ^{1}H{^{15}N} HSQC spectrum of the pH 5.0 solution of the NP2-NO complex is very well dispersed, as shown in Figure 2, red crosspeaks. Sequential assignments of the corresponding double-labeled NP2(D1A)-NO sample were made without any difficulty for all the non-proline residues except Ala1 and Gln171. However, 27 assigned peaks could not be included in the modelfree analysis calculations for the corresponding ^{15}N-labeled native N-terminus NP2-NO because their signal overlapped with that of another residue. This is in addition to the two residues that are unassigned and four proline residues that lack amide protons. Thus a total of 33 out of 179 residues were not included in the calculations.

The loop regions of special interest are the A-B loop and the G-H loop. All the residues in those two loops except Thr35 (A-B loop) and Asp128 (G-H loop) were assigned without any ambiguity, and did not overlap with other ^{15}N,^{1}H cross peaks, and were thus included in the modelfree analysis at pH 5.0. The E-F loop is also of interest, both because it is so long, and

---

[‡]Structures obtained at pH 5.6, PDB files 1SXW, 1ERX, 1IKJ, 1KOI, 1X8O, 1X8Q, 1SY1, 1SY3, 1YWA, 1YWB, 2AT0, 2AT5, 2AT6, 2AT8, but not 1D3S, 1IKE, 1EQD, 1SXU, 1SXX, 1SXY or 2AT3.

also because it is believed to be involved in the binding of NP2 (but no other *Rhodnius* NP) to Factor IX and IXa of the blood clotting cascade.[68-70] That is not the subject of this work, other than to note that the E-F loop shows similar dynamics to the A-B and G-H loops, although it is not involved in NO escape.

The R_1, R_2 and NOE values measured, along with the squared general order parameters (S^2) calculated at pH 5.0, are given in **Figure 4**. The R_1, R_2 and NOE values for all the residues are close in range to the average values, with few exceptions, mostly in the loop regions. The exceptions did not follow any pattern that would indicate correlated motions of either the A-B or G-H loop. For the modelfree analysis, the X-ray structure of the NP2(D1A) mutant of NP2 complexed with ammonia (PDB file 2EU7[8]), was chosen, because it is expected to have a similar loop structure to that of native N-terminus NP2, except for an as yet not understood special role for residue D1 that is not exhibited by A1 (this is evident from the differences in the kinetics of binding and release of NO from native N-terminus NP2, even though the ^{1}H NMR spectra of the two are so similar[17]), and it is one of the highest-resolution structures solved at pH 7.5. The initial estimate of the overall correlation time (τ_m) and the ratio of parallel to perpendicular rotational diffusion motional tensor, D_{ratio} ($D_{||}/D_{\perp}$) of the NP2-NO complex was calculated from the R_2/R_1 ratio using the program called *quadric_diffusion* (A.G. Palmer, Columbia University). This gave a value of 8.58 ns as the overall correlation time and a value of 0.91 as the D_{ratio}, which was used in the modelfree calculations. The relaxation data were analyzed with an axially symmetric diffusion tensor model based on the D_{ratio} value from the quadric diffusion analysis.[61]

The user-friendly program *FAST-Modelfree* (J. P. Loria, Yale University)[30] which interfaces with the *Modelfree program Ver. 4.1* (A. G. Palmer, Columbia University) was used to obtain the modelfree parameters. After the final rounds of optimization of the dynamic parameters, the D_{ratio} value was optimized to 1.09 for the NP2-NO complex, with $\tau_m = 8.61$ ns. The squared order parameters (S^2) are shown in Figure 4 and the model assigned for each residue is shown in Table 1 below. Out of 146 residues, 127 residues were best fit by Model 1, indicating no significant contribution from R_{ex} and local fast motions to the overall backbone relaxation. A total of 19 residues needed higher models to fit their relaxation data; nine residues were best fit by Model 2, which requires τ_e ; another set of four residues were best fit by Model 3, which requires S^2 and R_{ex}, and five other residues were best fit to Model 5, which requires S^2, S_f^2, and τ_e. Thus contribution from local motion and R_{ex} to the backbone relaxation is possible for only these 19 residues. All of those 19 residues are located in the loop regions, out of which only two residues D31 and S126 are located in the A-B or G-H loop. The S^2 values provide good information about the amplitude of picosecond-to-nanosecond local motions.[61] The typical order parameter observed in the structured regions of well-folded proteins is between 0.80 and 0.90 with an average value of 0.85, and is lower for flexible regions.[71] The S^2 values for all residues in the structured regions namely β-sheets and α-helices in this case are above the 0.85 average, indicating high rigidity of the molecule. Almost all the residues in the loop regions, with some exceptions, show lower values than 0.85, suggesting that the loop regions are flexible. A total of 14 residues (T4, I6, S7, G11, D13, K73, S76, S77, G78, D141, E143, Q158, S178 and L179) have S^2 values lower than 0.8, indicating that those residues are more flexible than others. It is interesting to note that the D-E loop (K73, S76, S77, G78) show flexibility and possibly correlated motion, but there is no evidence of any correlated motion in the A-B and G-H loops.

Similar analysis of the data obtained at pH 6.5 was carried out and the results are shown in Supporting Information Figure S9. Out of 146 residues used in the calculations, 118 residues were best fit by Model 1, suggesting no significant contributions from R_{ex} and local fast motions to the overall backbone relaxation. A total of 28 residues needed higher models to

fit their relaxation data; three residues were best fit by Model 2, which requires τ_e; another set of 12 residues were best fit by Model 3, which requires S^2 and R_{ex}; one residue was best fit to model 4, which requires S^2, τ_e, and R_{ex}, and the other 10 residues were best fit to Model 5, which requires S^2, S_f^2, and τ_e. Similar to the pH 5 results, those 28 residues which require higher models to fit the relaxation data are located in the loop regions, with some exceptions. Those exceptions are residues D13, C39, F66, K73, E110, D131 and Y133, which are located in various parts of structured regions, i.e. either in an α-helix or in a β-sheet. The observation of S^2 values above 0.85 for almost all of the α-helical as well as β-sheet regions suggests that they are rigid. The D-E loop (residues 75-78) and the loop region after β_H (residues 139-143) exhibit high degrees of flexibility, as evidenced from their reduced S^2 values and the need for higher models to fit the relaxation data.

At pH 7.3, all but eight non-proline residues were assigned. However, many ^{15}N,^1H crosspeaks have moved significantly compared to the pH 5 spectrum. Though the number of overlapped peaks remained almost the same at this high pH value, many of the overlapped resonances are different from those which overlapped at pH 5. It is noteworthy that the resonances of the A-B and G-H loop regions of the protein showed pH-dependent perturbation of their chemical shifts, as discussed above and shown in Figure 3. In the modelfree analysis, these eight residues, plus 22 others, were not included, because either the signals overlap, or they have very low intensity in the $^1H\{^{15}N\}$ HSQC spectrum. The R_1, R_2 and NOE values measured at pH 7.3 are given in **Figure 5**, along with the calculated order parameters, S^2. The R_1 values for all the residues fall within the range of the average value of all residues. However, four residues in the A-B loop (D29, D31, Q33, V34) showed dramatic pH-dependent R_2 rate increases. The other residues which show higher R_2 are D14, C39, S40, D128 and K140. The significant increases in R_2, strongly suggest that these residues undergo μs-ms time scale dynamics at pH 7.3, in contrast to the results seen at pH 5.0 and 6.5.

The *quadric_diffusion* analysis using the R_2/R_1 ratio yielded an initial estimate of the overall molecular correlation time (τ_m) of 8.8 ns with a D_{ratio} ($D_{//}/D_{\perp}$) value of 0.89. After the final rounds of optimization of the dynamic parameters, the D_{ratio} value was optimized to 0.95, with a τ_m of 8.41 ns. In contrast to the pH 5.0 and pH 6.5 results, as many as 35 residues at pH 7.3 needed higher models to fit the experimental relaxation parameters, and interestingly, all the assigned residues in the A-B loop needed higher models. The A-B loop region of NP2 consists of 10 residues, which include one proline. Backbone assignments for K30 and T35, which are present in the A-B loop, were not possible. Out of 7 residues assigned in the A-B loop, 4 residues (D29, D31, Q33, and V34) required Model 4 to fit the data, one residue (D36) required Model 2, and one other residue (Q37) required Model 3, indicating the possibility of significant contribution from R_{ex} and local motions to their backbone relaxation.

The G-H loop, which is also believed to be involved in NO release,[10] does not show any of the trends seen for the A-B loop. Only residue D128 showed an increase in R_2, and Model 3 was needed to fit the relaxation data, suggesting contribution of local motion and conformational exchange for this residue at pH 7.3. However this cannot be compared with the pH 5.0 and 6.5 results because this residue was not included in the modelfree analysis at pH 5.0 or 6.5 because of signal overlap. The dependence of τ_m on residue number at each of the three pH values is shown in Supporting Information Figure S9, where it can be seen that for the majority of the protein, the τ_m value is quite constant, except for the residues of the A-B loop at pH 7.3.

A summary comparison of the relaxation data for the A-B and G-H loops at pH 5.0 and 7.3 is shown in **Figure 6**, where it can clearly be seen that the R_1 data do not vary significantly

with pH, while the R_2 and NOE data vary significantly. Observation of lower NOE values for the residues in the A-B loop (<0.6) also suggests a local flexibility of the protein on the picosecond to nanosecond time scale. Thus, the modelfree results for the pico- to nanosecond dynamics, like the chemical shift changes observed over the same pH range (Figure 3), clearly suggest that at least the A-B loop undergoes dynamic motions at pH 7.3.

The trend of the S^2 values for pH 7.3 follows similar trends (rigid) seen for the lower pH results, as far as the structured regions (α-helices and β-sheets) are concerned, with few exceptions. But for the loop regions there are two significant differences observed. The D-E loop, which is flexible at lower pH values, becomes rigid at this higher pH value. Most importantly, the A-B loop, which is believed to be involved in the NO binding/release mechanism,[10,19] is shown to be flexible at this higher pH value, but was rigid at both pH 5.0 and 6.5.

Slow time scale dynamics.

Transverse relaxation (T_2) measurements using the Carr-Purcell-Meiboom-Gill (CPMG) pulse sequence have emerged as a very powerful method for studying the slow timescale motions (microseconds to milliseconds) in protein dynamics.[34,35] To probe backbone motions of the NP2-NO complex occurring in these slow timescales, effective transverse ^{15}N relaxation rates (R_2^{eff}) were recorded as a function of CPMG field strength (ν_{CPMG}) at three different pH values. The data were analyzed using the software NESSY.[65] The program found best fits for almost all the residues as Model 1, meaning R_2^{eff} are not dependent on the CPMG field. In other words, the dispersion curves are flat: there were no CPMG field-dependent peak intensity changes observed. Model 1 of the relaxation dispersion experiments does not involve the R_{ex} term in the equation, *i.e.* $R_2^{eff} = R_2^0$. We have also calculated per residue two point $\Delta R_2^{eff}(\nu_{CPMG})$ values for the NP2-NO complex using Equation 1 given in the Experimental Section. The results are shown in **Figure 7**. This approach has been very well utilized to probe the hydrogen-bonding network in a bacterial heme oxygenase enzyme.[72] In general, $\Delta R_2^{eff}(\nu_{CPMG})$ is positive for those residues with μs-ms conformational exchange. In the absence of μs-ms conformational exchange, $\Delta R_2^{eff}(\nu_{CPMG})$ becomes zero, as there is no CPMG field-dependent peak intensity change. The $\Delta R_2^{eff}(\nu_{CPMG})$ values are close to zero for almost all residues in the NP2-NO complex at all pH values, except for a few residues; C39, K140, G156 and T177 at pH 5.0, C39, S40, K140 and D141 at pH 6.5 and D29, V34, S77 and S114 at pH 7.3. It is interesting to note that at pH 7.3 residues D29 and V34, located in the A-B loop, are consistent with the modelfree analysis on the fast timescales, and also show evidence of μs-ms conformational exchange. On the other hand, the pH 5 and 6.5 results show that the residues with evidence of μs-ms conformational exchange are scattered in the protein sequence and do not include residues of the A-B loop. The scattered nature of the residues showing μs to ms dynamics seen for NP2-NO, even at pH 7.3, confirms the rigid nature of this β-barrel protein and indicates that motions are localized, and are not indicative of correlated, total loop motions.

Discussion

As can be seen from the results obtained in this study, the diamagnetic NO complex of nitrophorin 2, NP2-NO, is fairly rigid on all timescales, although it shows somewhat more dynamics at pH 7.3 than at either pH 6.5 or 5.0. Based on chemical shift changes between pH 5.0 and 7.3, it appears that the A-B loop shows some small changes in conformation, but at both pH values there are differences from that observed in the crystal structure obtained at pH 7.5 for NP2(D1A)-NH$_3$, PDB file 2EU7.[8]

The mechanisms of NO binding and release have been probed by computational methods by two groups.[73-76] Kondrashov and Montfort carried out comparative nonequilibrium

molecular dynamics (MD) simulations on NP4-NO at pH 5 and 7 and of Mb-NO,[73] while the Argentine group of Estrin carried out both MD and hybrid quantum mechanics/ molecular mechanics (QM/MM) calculations to learn about the dynamics of NP4 and to analyze the Fe-NO bond strength at pH 5.6 and 7.4.[74] It was reported that the Fe-NO bond strength in the two NP4 loop conformations is the same, and thus NO escape from NP4 is determined by differential NO migration rates rather than by a different Fe-NO bond strength at the two pH values.[74] They treated NO escape as a two-state model, opened and closed. More recently, the Argentine group carried out MD calculations on NP2 as compared to NP4.[75] These computational studies suggest that loop opening and closing are primarily responsible for the rate of NO binding and release. However, this does not appear to be a two-state process, because there are many structures of NP4 and its ligand complexes that show *partially open* or *partially closed* A-B and G-H loops,[10-14] and recent work by Montfort et al. stresses the fact that both conformations are present at all pH values, but that the fraction of each varies with pH.[23]

More recently, the Argentine group carried out MD calculations on NP2 and NP4.[75] They found that NP2 undergoes a much smaller change in conformation of the A-B and G-H loops as a function of pH, and that at low pH, the only escape route from the distal pocket of NP2 is a high-energy route passing between the staves of the β-barrel.[75] However, those calculations were done on PDB files which have M0 present, where closure of the A-B loop is prevented by the large methionine side chain.[18] A better PDB file to have used would have been that for NP2(D1A)-NH$_3$ (PDB file 2EU7), which we have used for analysis of the NMR dynamics data. Instead, the PDB files 1EUO and 2AL0, (M0)NP2-NH$_3$ and (M0)NP2(Fe(II))-H$_2$O, respectively, were used;[75] the 2AL0 structure has the space group $P4_12_12^8$, which also contains a disordered citrate molecule in between the two proteins at the site of one of the heme carboxylates. Besides the heme carboxylate, the citrate interacts through hydrogen-bonds with Tyr85, Lys96, Asn102, and Glu124 of the two molecules. The Glu124 carboxylates of the two molecules also hydrogen-bond to each other. The strong interactions between pairs of molecules in the unit cell appear to distort the G-H loops of the two molecules, thus possibly leading to erroneous conclusions from the MD calculations.

The most recent publication from the Argentine group is mainly focused on calculation of the pK_a of Asp30 of NP4 as a function of pH. All of the publications on NP4-NO kinetics[19-24] and their theoretical treatments[73-76] have focused mainly on Asp30 and its hydrogen-bond to Leu130 C=O. As mentioned in the introduction, the deprotonation of Asp30 breaks that hydrogen-bond, which is believed to cause the A-B and G-H loops to open and allow NO to escape. This most recent paper from the Argentine group discusses the fact that from computations they can show that Asp30 has two micro-pK_as, that with the hydrogen-bond present being 8.5 (the "closed" conformation), and the other, with the hydrogen-bond absent, being 4.3 (the "open" conformation).[76] The measured thermodynamic pK_a that is believed to be associated with Asp30 is about 6.5,[19] which is close to the midpoint between these micro-pK_a values.[76] The pK_a of D30 of NP4 has been estimated to be 5.5 ± 0.4[77] (and that of the D29 of NP2 5.4 ± 0.4[77]), both estimated from the pH dependence of the midpoint potential of the D30A mutant of NP4 (and the D29A mutant of NP2).[77] However, no consideration of an important role for the homodimer of NP4 was included in these studies.

Viewed in those contexts, the loop structure, detected by changes in the chemical shifts of backbone atoms of NP2-NO between pH 5.0 and 7.3, Figure 3, and their expected values for helical, β-sheet or random coil sequences at pH 5.0, where the protein is quite rigid, is consistent with the slow rate of dissociation of NO at that pH ($k_{off} = 0.030 ± 0.002$ s^{-1}).[17] The loop structure at pH 7.3 is somewhat different, with individual amino acids of the A-B loop undergoing dynamic motions, but there is no evidence of a large conformational

change of the loops as a function of pH. The greater dynamic motions at pH 7.3 are consistent with a somewhat faster rate of dissociation of NO at that higher pH (k_{off} = 0.093 ± 0.002 s^{-1}),[17] but this is only a factor of three faster than at pH 5.0.[17] As mentioned above, most (but not all) NP4-NO structures at pH 5.6 (PDB file 1KOI, for example) show a partially helical A-B loop structure, which is different from the less distinct helix predicted herein for NP2 from analysis of the NMR chemical shifts at low pH. Also, NP4 has two prolines in the A-B loop, five residues apart; the observed short helix begins with the first Pro. The second Pro is not involved. It should also be noted that the NO complex of NP2 was expected to be particularly rigid, based on the pH 5.6 structures obtained for monomeric NP4-NO,[9-14] as compared to the high-pH structures of NP4 bound to other ligands,[4,5,9-12] and NP2 structures at pH 6.5 and 7.5.[7,8] The dynamics of the high-spin aqua complexes of NP2 and NP4 are currently under study in our laboratory.

A question asked by the reviewers of this paper is: Why did we not do H/D exchange studies of the amide protons of NP2-NO, since it could be that this might be a way of observing slower motions that are involved with loop opening and closing, and thus NO escape? In fact, we have carried out H/D exchange studies on apo-NP2 (Filippov, I., unpublished results). These studies show the amide protons of the A-B, and G-H loop residues of interest exchange too rapidly to be measured ($t_{1/2}$ < 3 min, as would be expected for solvent-exposed loops and consistent with the seconds timescale observed for NO dissociation ($t_{1/2}$ values of about 23 s and 7 s, at pH 5.0 and 7.5, respectively[17]), since it would be reasonable to expect the loops to open and close a number of times before the NO molecule would both be free from the iron and have the right trajectory to escape through the open loop conformation. Initial studies on the holo-NP2-NO complex are also consistent with this, with the side-chains of interest all completely exchanged (or nearly so in the case of D36) by the first acquisition (Berry, R. E. and Muthu, D., unpublished).

The dynamics of several other lipocalins and some of the subset of fatty acid binding proteins and the related bile acid binding proteins have been investigated on the pico- to nanosecond and micro- to millisecond timescales, and in general, these proteins have invariably been shown to be fairly rigid,[43,78-86] because the β-barrel structure imparts strong controls over the flexibility of the protein, in comparison to mainly α-helical proteins. Some β-barrel proteins show somewhat more dynamics than does NP2-NO, while others show very comparable dynamics. Some of the earliest studies of backbone mobility and conformational flexibility have been carried out on the fatty acid subclass of lipocalins (β_A-α_I-α_{II}-β_B-β_C-...-β_H): For the rat intestinal fatty acid-binding protein, the majority of the residues in both the apo- and holoprotein were characterized by relatively slow hydrogen exchange rates, high generalized order parameters, and no conformational exchange terms. However, helix II and the C-D and E-F loops of the apoprotein showed rapid hydrogen exchange, low order parameters and significant conformational exchange. The unique behavior of these parts of the apoprotein is believed to permit entry of the fatty acid into the binding cavity.[78]

Another of the early lipocalins to be studied is β-lactoglobulin, a 162-residue protein found in copious quantities in the whey fraction of the milk of ruminants and other species, but not in human milk. Although its specific role is not known, it is capable of binding small hydrophobic molecules including fatty acids,[79,80] retinol,[80,81] protoporphyrin IX[81] and others. β-Lactoglobulin is dimeric at physiological pH,[82] but is monomeric below pH 3. The group of Goto[83] carried out NMR studies of the structure and dynamics of the monomeric form of the A variant of the protein at pH 2.0 and 45 °C, and the group of Barlow[84] has studied the same variant at pH 2.6 and 37 °C. Both studies found most of the protein to be quite rigid in the pico- to nanosecond timescales, with the exception of the loops. But as we

have also found for NP2-NO, only individual residues exhibit signs of dynamics on the micro- to millisecond timescale, rather than entire loops.

Finally, the bile acid-binding proteins, previously called "liver basic" fatty acid binding proteins, are 10-stranded β-barrel proteins of the same general design as the 8-stranded β-barrel fatty acid binding proteins proteins (β_A-α_I-α_{II}-β_B-β_C-...-β_J), which tend to bind two molecules of bile salts such as glycocholic acid or glycochenodeoxycholic acid, or both. Two groups have reported dynamics studies of these systems, Molinari et al.[85] and Toke et al.[43] Molinari et al. determined the structure of the chicken liver bile acid-binding apoprotein and obtained the ^{15}N relaxation times and steady-state $^{15}N\{^1H\}$ NOE data of the apoprotein at pH 5.6 and 7.0, and of the holoprotein at pH 7.0 bound to chenodeoxycholate. The modelfree relaxation studies were performed at three different magnetic fields, corresponding to 500, 600 and 700 MHz for the proton, at 298 K.[85] The paper of Toke et al.[43] is the most thorough study of the dynamics of a β-barrel protein reported thus far. Measurements of the internal motions and exchange processes involved in human ileal bile acid binding protein were made at 600 and 400 MHz. Samples included the apo- and the holoprotein, which was prepared with ratios 1:1.5:1.5 of protein:cholic acid: chenodeoxycholic acid. Five representations of the spectral density function were considered in analyzing the results, as we have also considered (Table 1). The results of the modelfree analysis showed that 84 of the residues of the apo- and 85 of the holoprotein behaved according to Model 1, 11 of both apo- and holoprotein behaved according to Model 2, 11 of the apo- and 9 of the holoprotein behaved according to Model 3, none of the residues of either apo- or holoprotein behaved according to Model 4, and 8 residues of the apo- and 9 of the holoprotein required Model 5. Relaxation dispersion NMR experiments indicate a marked difference between the two protein states on the μs-ms timescale.[43]

In conclusion, NP2-NO is not alone among lipocalins in being a fairly rigid protein, and it is obvious that in contrast to the large motions of well-described two-state protein structures analyzed in detail by Kay and coworkers,[32-39] the dynamics of lipocalins are far more subtle, and are very pH-dependent. Nevertheless, close scrutiny of the results of modelfree and CPMG experiments clearly show that even proteins described as "highly rigid" undergo motions that allow binding and release of ligands on biologically relevant timescales without undergoing concerted, large scale motions. And in most cases, the ligand-free forms exhibit greater dynamics than the ligand-bound forms. Preliminary investigations of the dynamics of the NO-off form of NP2 and those of the NO-off form of NP4 are in progress, and in both cases significantly more dynamics are observed, more for NP4 than for NP2.[87] Detailed reports of these investigations will be presented when the studies have been completed. However, the extreme stability of the homodimeric form of NP4-NO, even at pH 7.3 and 0.2 mM (Berry, R. E., unpublished work), precludes comparative studies to those reported herein.

Supplementary Material

Refer to Web version on PubMed Central for supplementary material.

Acknowledgments

References

1. Ribeiro JMC, Hazzard JMH, Nussenzveig RH, Champagne DE, Walker FA. Reversible Binding of Nitric Oxide by a Salivary Heme Protein from a Blood-sucking Insect. Science. 1993; 260:539–541. [PubMed: 8386393]

2. Champagne DE, Nussenzveig R, Ribeiro JMC. Purification, Partial Characterization, and Cloning of Nitric Oxide-carrying Heme proteins (Nitrophorins) from Salivary Glands of the Blood-sucking Insect *Rhodnius prolixus*. J. Biol. Chem. 1995; 270:8691–8695. [PubMed: 7721773]

3. Walker FA. Nitric Oxide Interaction with Insect Nitrophorins, and Thoughts on the Electron Configuration of the {FeNO}^{6} Complex. J. Inorg. Biochem. 2005; 99:216–236. [PubMed: 15598503]

4. Weichsel A, Andersen JF, Champagne DE, Walker FA, Montfort WR. Crystal Structures of a Nitric Oxide Transport Protein from a Blood-Sucking Insect. Nat. Struct. Biol. 1998; 5:304–309. [PubMed: 9546222]

5. Ding XD, Weichsel A, Balfour C, Shokhireva TK, Pierik A, Averill BA, Mont-fort WR, Walker FA. Nitric Oxide Binding to the Ferri- and Ferroheme States of Nitrophorin 1, a Reversible NO-Binding Heme Protein from the Saliva of a Blood-Sucking Insect, *Rhodnius prolixus*. J. Am. Chem. Soc. 1999; 121:128–138.

6. Berry RE, Ding XD, Shokhireva TK, Weichsel A, Montfort WR, Walker FA. Axial Ligand Complexes of the Rhodnius Nitrophorins: Electrochemistry, Binding Constants, and Structures of the 4-Iodopyrazole and Imidazole Complexes of NP4. J. Biol. Inorg. Chem. 2004; 9:135–144. [PubMed: 14673714]

7. Andersen JF, Montfort WR. The Crystal Structure of Nitrophorin 2, A Trifunctional Antihemostatic Protein from the Saliva of *Rhodnius prolixus*. J. Biol. Chem. 2000; 275:30496–30503. [PubMed: 10884386]

8. Weichsel A, Berry RE, Zhang H, Walker FA, Montfort WR. Crystal Structures, Conformational Change and Heme Deformation in Complexes of Nitrophorin 2, a Nitric Oxide Transport Protein from *Rhodnius prolixus*. PDB files available: http://www.rcsb.org/. : 1PEE, 1PM1, 1T68, 2A3F, 2ACP, 2AH7, 2AL0, 2ALL, 2AMM, 2ASN, 2EU7, 2HYS, 2GTF.

9. Andersen JF, Weichsel A, Balfour C, Champagne DE, Montfort WR. The Crystal Structure of Nitrophorin 4 at 1.5 Å Resolution: Transport of Nitric Oxide by a Lipocalin-Based Heme Protein. Structure. 1998; 6:1315–1327. [PubMed: 9782054]

10. Weichsel A, Andersen JF, Roberts SA, Montfort WR. Nitric Oxide Binding to Nitrophorin 4 Induces Complete Distal Pocket Burial. Nat. Struct. Biol. 2000; 7:551–554. [PubMed: 10876239]

11. Roberts SA, Weichsel A, Qiu Y, Shelnutt JA, Walker FA, Montfort WR. Ligand-Induced Heme Ruffling and Bent NO Geometry in Ultra-High-Resolution Structures of Nitrophorin 4. Biochemistry. 2001; 40:11327–11337. [PubMed: 11560480]

12. Maes EM, Weichsel A, Andersen JF, Shepley D, Montfort WR. Role of Binding Site Loops in Controlling Nitric Oxide Release: Structure and Kinetics of Mutant Forms of Nitrophorin 4. Biochemistry. 2004; 43:6679–6690. [PubMed: 15157102]

13. Maes EM, Roberts SA, Weichsel A, Montfort WR. Ultrahigh Resolution Structures of Nitrophorin 4: Heme Distortion in Ferrous CO and NO Complexes. Biochemistry. 2005; 44:12690–12699. [PubMed: 16171383]

14. Kondrashov DA, Roberts SA, Weichsel A, Montfort WR. Protein Functional Cycle Viewed at Atomic Resolution: Conformational Change and Mobility in Nitrophorin 4 as a Function of pH and NO Binding. Biochemistry. 2004; 43:13637–13647. [PubMed: 15504026]

15. Yuda M, Hirai M, Miura K, Matsumura H, Ando K, Chinzei Y. cDNA Cloning, Expression and Characterization of Nitric-Oxide Synthase from the Salivary Glands of the Blood-Sucking Insect *Rhodnius prolixus*. Eur. J. Biochem. 1996; 242:807–812. [PubMed: 9022713]

16. Poulos TL. Soluble guanylate cyclase. Curr. Opin. Struct. Biol. 2006; 16:736–743. [PubMed: 17015012]

17. Berry RE, Muthu D, Garrett SA, Shokhireva TK, Zhang H, Walker FA. Native N-Terminus Nitrophorin 2 from the Kissing Bug: Similarities to and Differences from NP2(D1A). Chem. Biodiv. 2012; 9:1739–1755.

18. Berry RE, Shokhireva T, Filippov I, Shokhirev MN, Zhang H, Walker FA. Effect of the N-Terminus on Heme Cavity Structure, Ligand Equilibrium, Rate Constants, and Reduction Potentials of Nitrophorin 2 from *Rhodnius prolixus*. Biochemistry. 2007; 46:6830–6843. [PubMed: 17506528]

19. Andersen JF, Ding XD, Balfour C, Champagne DE, Walker FA, Montfort WR. Kinetics and Equilibria in Ligand Binding by Nitrophorins 1-4: Evidence for Stabilization of a NO-Ferriheme Complex through a Ligand-Induced Conformational Trap. Biochemistry. 2000; 39:10118–10131. [PubMed: 10956000]

20. Nienhaus K, Maes EM, Weichsel A, Montfort WR, Nienhaus GU. Structural Dynamics Controls Nitric Oxide Affinity in Nitrophorin 4. J. Biol. Chem. 2004; 279:39401–39407. [PubMed: 15258143]

21. Kubo M, Gruia F, Benabbas A, Barabanschikov A, Montfort WR, Maes EM, Champion PM. Low-Frequency Mode Activity of Heme: Femtosecond Coherence Spectroscopy of Iron Porphine Halides and Nitrophorin. J. Am. Chem. Soc. 2008; 130:9800–9811. [PubMed: 18597456]

22. Benabbas A, Ye X, Kubo M, Zhang Z, Maes EM, Montfort WR, Champion PM. Ultrafast Dynamics of Diatomic Ligand Binding to Nitrophorin 4. J. Am. Chem. Soc. 2010; 132:2811–2820. [PubMed: 20121274]

23. Cheng M, Brookes JP, Montfort WR, Khalil M. pH-Dependent Picosecond Structural Dynamics in the Distal Pocket of Nitrophorin 4 Investigated by 2D IR Spectroscopy. J. Phys. Chem. B. 2013 DOI: 10.1021/jp407052a.

24. Abbruzzetti S, He C, Ogata H, Bruno S, Viappiani C, Knipp M. Heterogeneous Kinetics of the Carbon Monoxide Association and Dissociation Reaction to Nitrophorin 4 and 7 Coincide with Structural Heterogeneity of the Gate-Loop. J. Am. Chem. Soc. 2012; 134:9986–9998. [PubMed: 22594621]

25. Berry RE, Muthu D, Shokhireva TK, Garrett SA, Goren AM, Zhang H, Walker FA. NMR Investigations of Nitrophorin 2 Belt Side Chain Effects on Heme Orientation and Seating of Native N-Terminus NP2 and NP2(D1A). J. Biol. Inorg. Chem. 2013 in press.

26. Lipari G, Szabo A. Model-free Approach to the Interpretation of Nuclear Magnetic Resonance Relaxation in Macromolecules. 1. Theory and Range of Validity. J. Am. Chem. Soc. 1982; 104:4546–4559.

27. Lipari G, Szabo A. Model-free Approach to the Interpretation of Nuclear Magnetic Resonance Relaxation in Macromolecules. 2. Analysis of Experimental Results. J. Am. Chem. Soc. 1982; 104:4559–4570.

28. Clore GM, Driscoll PC, Wingfield PT, Gronenborn AM. Analysis of Backbone Dynamics of Interlukin 1β Using Two-dimensional Inverse Detected Heteronuclear ^{15}N-^{1}H NMR Spectroscopy. Biochemistry. 1990; 29:7387–7401. [PubMed: 2223770]

29. Clore GM, Szabo A, Bax A, Kay LE, Driscoll PC, Gronenborn AM. Deviations from the Simple Two Parameter Model Free Approach to the Interpretation of ^{15}N Nuclear Magnetic Relaxation of Proteins. J. Am. Chem. Soc. 1990; 112:4989–4991.

30. Farrow NA, Muhandham JR, Singer AJ, Pascal SM, Kay CM, Gish G, Shoelson SE, Pawson T, Forman-Kay JD, Kay LE. Backbone Dynamics of a Free and a Phosphopeptide-Complexed Src Homology 2 Domain Studied by ^{15}N NMR Relaxation. Biochemistry. 1994; 33:5984–6003. [PubMed: 7514039]

31. Cole R, Loria JP. FAST-Modelfree: A Program for Rapid Automated Analysis of Solution NMR Spin-Relaxation Data. J. Biomol. NMR. 2003; 26:203–213. [PubMed: 12766418]

32. Mulder FAA, Hon B, Muhandiram DR, Dahlquist FW, Kay LE. Flexibility and Ligand Exchange in a Buried Cavity Mutant of T4 Lysozyme Studied by Multi-nuclear NMR. Biochemistry. 2000; 39:12614–12622. [PubMed: 11027141]

33. Tollinger M, Skrynnikov NR, Mulder FAA, Forman-Kay JD, Kay LE. Slow Dynamics in Folded and Unfolded States of an SH3 Domain. J. Am. Chem. Soc. 2001; 123:11341–11352. [PubMed: 11707108]

34. Korzhnev DM, Kay LE. Probing Invisible, Low-Populated States of Protein Molecules by Relaxation Dispersion NMR Spectroscopy: An Application to Protein Folding. Acc. Chem. Res. 2008; 41:442–451. [PubMed: 18275162]

35. Palmer AG. NMR Characterization of the Dynamics of Biomacromolecules. Chem. Rev. 2004; 104:3623–3640. [PubMed: 15303831]
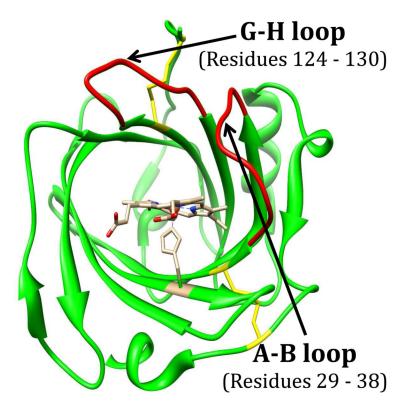
36. Eisenmesser EZ, Millet O, Labeikovsky W, Korzhnev DM, Wolf-Watz M, Bosco DA, Skalickey JJ, Kay LE, Kern D. Intrinsic Dynamics of an Enzyme Underlies Catalysis. Nature. 2005; 438:117–121. [PubMed: 16267559]

37. Boehr DD, McElheny D, Dyson HJ, Wright PE. The Dynamic Energy Landscape of Dihydrofolate Reductase Catalysis. Science. 2006; 313:1638–1642. [PubMed: 16973882]

38. Korzhnev DM, Religa TL, Banachewicz W, Fersht AR, Kay LE. A Transient and Low-Populated Protein-Folding Intermediate at Atomic Resolution. Science. 2010; 329:1312–1316. [PubMed: 20829478]

39. Bouvignies G, Hansen DF, Vallurupalli P, Kay LE. Divided-Evolution-Based Pulse Scheme for Quantifying Exchange Processes in Proteins: Powerful Complement to Relaxation Dispersion Experiments. J. Am. Chem. Soc. 2011; 133:1935–1945. [PubMed: 21244030]

40. Morin SB. A Practical Guide to Protein Dynamics from ^{15}N Spin Relaxation in Solution. Prog. NMR Spectrosc. 2011; 59:245–262.

41. Kleckner IR, Foster MP. An Introduction to NMR-based Approaches for Measuring Protein Dynamics. Biochim. Biophys. Acta - Proteins and Proteomics. 2011; 1814:942–968.

42. Torbeev VY, Raghuraman H, Hamelberg D, Tonelli M, Westler WM, Perozo E, Kent SBH. Protein Conformational Dynamics in the Mechanism of HIV-1 Pro-tease Catalysis. Proc. Natl. Acad. Sci. U.S.A. 2011; 108:20982–20987. [PubMed: 22158985]

43. Horváth G, Király P, Tárkányi G, Toke O. Internal Motions and Exchange Processes in Human Ileal Bile Acid Binding Protein As Studied by Backbone ^{15}N Nuclear Magnetic Resonance Spectroscopy. Biochemistry. 2012; 51:1848–1861. [PubMed: 22329738]

44. Marley J, Lu M, Bracken C. A Method for Efficient Isotopic Labeling of Recombinant Proteins. J. Biomol. NMR. 2001; 20:71–75. [PubMed: 11430757]

45. Neidhardt FC, Bloch PL, Smith DF. Culture Medium for Enterobacteria. J. Bacteriol. 1974; 119:736–747. [PubMed: 4604283]

46. Abriata LA, Zaballa M-E, Berry RE, Yang F, Zhang H, Walker FA, Vila AJ. Electron Spin Density on the Axial His Ligand of High-Spin and Low-Spin Nitrophorin 2 Probed by Heteronuclear NMR Spectroscopy. Inorg. Chem. 2013; 52:1285–1295. [PubMed: 23327568]

47. Andersen JF, Champagne DE, Weichsel A, Ribeiro JMC, Balfour CA, Dress V, Montfort WR. Nitric Oxide Binding and Crystallization of Recombinant Nitrophorin 1, a Nitric Oxide Transport Protein from the Blood-Sucking Bug *Rhodnius prolixus*. Biochemistry. 1997; 36:4423–4428. [PubMed: 9109649]

48. Buchner J, Pastan I, Brinkmann U. A Method for Increasing the Yield of Properly Folded Recombinant Fusion Proteins: Single-chain Immunotoxins from Renaturation of Bacterial Inclusion Bodies. Analytical Biochemistry. 1992; 205:263–270. [PubMed: 1332541]

49. Zhang X, Cardosa L, Broderick M, Fein H, Davies IR. Novel Calibration Method for Nitric Oxide Microsensors by Stoichiometrical Generation of Nitric Oxide from SNAP Electroanal. Chem. 2000; 12:425–428.

50. Bahrami A, Assadi AH, Markley JL, Eghbalnia HR. Probabilistic Interaction Network of Evidence Algorithm and Its Application to Complete Labeling of Peak Lists from Protein NMR Spectroscopy. PLoS Comput. Biol. 2009 Mar. 2009; 5(3):e1000307.

51. Lee W, Westler WM, Bahrami A, Eghbalnia HR, Markley JL. PINE-SPARKY: Graphical Interface for Evaluating Automated Probabilistic Peak Assignments in Protein NMR Spectroscopy. Bioinformatics. 2009; 25:2085–7. [PubMed: 19497931]

52. Markley JL, Bax A, Arata Y, Hilbers CW, Kaptein R, Sykes BD, Wright PE, Wüthrich K. Recommendations for the Presentation of NMR Structures of Proteins and Nucleic Acids. Eur. J. Biochem. 1998; 256:1–15. [PubMed: 9746340]

53. Cornilescu G, Delaglio F, Bax A. Protein Backbone Angle Restraints from Searching a Database for Chemical Shift and Sequence Homology. J. Biomol. NMR. 1999; 13:289–302. [PubMed: 10212987]

54. Shen Y, Delaglio F, Cornilescu G, Bax A. TALOS+: A Hybrid Method for Predicting Protein Backbone Torsion Angles from NMR Chemical Shifts. J. Biomol. NMR. 2009; 44:213–223. [PubMed: 19548092]

55. Shen Y, Bax A. Protein Backbone and Sidechain Torsion Angles Predicted from NMR Chemical Shifts Using Artificial Neural Networks. J. Biomol. NMR. 2013; 56:227–241. [PubMed: 23728592]

56. Berjanskii MV, Wishart DS. A Simple Method To Predict Protein Flexibility Using Secondary Chemical Shifts. J. Am. Chem. Soc. 2005; 127:14970–14971. [PubMed: 16248604]

57. Delaglio F, Grzesiek S, Vuister GW, Zhu G, Pfeifer J, Bax A. NMRPipe: A Multidimensional Spectral Processing System Based on UNIX Pipes. J. Biomol. NMR. 1995; 6:277–293. [PubMed: 8520220]

58. Delaglio, F. NMRPipe: A Comprehensive Software System for Multidimensional NMR Applications. 2006-2012. http://www.nmrscience.com/nmrpipe.html

59. Goddard, TD.; Kneller, DG. SPARKY 3, Version 3.115, last revised May 30, 2008. University of California; San Francisco: http://www.cgl.ucsf.edu/home/sparky/

60. Cole, Roger; Patrick Loria, J. Department of Chemistry, Yale University; P.O. Box 208107, New Haven, CT 06520, U.S.A.:

61. Mandel AM, Akke M, Palmer AG. Backbone Dynamics of Escherichia coli Ribonuclease HI - Correlations with Structure and Function in an Active Enzyme. J. Mol. Biol. 1995; 246:144–163. [PubMed: 7531772]

62. Brüschweiler R, Liao X, Wright PE. Long-range motional restrictions in a multi-domain zinc-finger protein from anisotropic tumbling. Science. 1995; 268:886–889. [PubMed: 7754375]

63. Lee AL, Urbauer JL, Wand AJ. Improved labeling strategy for ^{13}C relaxation measurements of methyl groups in proteins. J. Biomol. NMR. 1997; 9:437–440. [PubMed: 9255947]

64. Pettersen EF, Goddard TD, Huang CC, Couch GS, Greenblatt DM, Meng EC, Ferrin TE. UCSF Chimera-a visualization system for exploratory research and analysis. J. Comput. Chem. 2004; 25:1605–1612. [PubMed: 15264254]

65. Bieri M, Gooley PR. Automated NMR Relaxation Dispersion Data Analysis Using NESSY. BMC Bioinformatics. 2011; 12:421. [PubMed: 22032230]

66. Morin SB. A Practical Guide to Protein Dynamics from ^{15}N Spin Relaxation in Solution. Prog. NMR Spectrosc. 2011; 59:245–262. 2011.

67. Kleckner IR, Foster MP. An Introduction to NMR-based Approaches for Measuring Protein Dynamics. Biochem. Biophys. Acta - Proteins and Proteomics. 2011; 1814:942–968.

68. Andersen JF, Gudderra NP, Francischetti IMB, Ribeiro JMC. The Role of Salivary Lipocalins in Blood Feeding by *Rhodnius prolixus*. Arch. Insect Biochem. Physiol. 2005; 58:97–105. [PubMed: 15660358]

69. Gudderra NP, Ribeiro JMC, Andersen JF. Structural Determinants of Factor IX(a) Binding in Nitrophorin 2, a Lipocalin Inhibitor of the Intrinsic Coagulation Pathway. J. Biol. Chem. 2005; 280:25022–25028. [PubMed: 15866866]

70. Mizurini DM, Francischetti IMB, Andersen JF, Monteiro RQ. Nitrophorin 2, a Factor IX(a)-directed Anticoagulant, Inhibits Arterial Thrombosis without Impairing Haemostasis. Thromb. Haemost. 2010; 104:1116–1123. [PubMed: 20838739]

71. Kempf JG, Loria JP. Protein Dynamics from Solution NMR: Theory and Applications. Cell Biochem. Biophys. 2003; 37:187–211. [PubMed: 12625627]

72. Zeng Y, Wilks A, Rivera M. The Hydrogen-Bonding Network in Heme Oxygen-ase Also Functions as a Modulator of Enzyme Dynamics: Chaotic Motions upon Disrupting the H-Bond Network in Heme Oxygenase from *Pseudomonas aeruginosa*. J. Am. Chem. Soc. 2007; 129:11730–11742. [PubMed: 17764179]

73. Kondrashov DA, Montfort WR. Nonequilibrium Dynamics Simulations of Nitric Oxide Release: Comparative Study of Nitrophorin and Myoglobin. J. Phys. Chem. B. 2007; 111:9244–9252. [PubMed: 17622170]

74. Marti MA, Lebrero MCG, Roitberg AE, Estrin DA. Bond or Cage Effect: How Nitrophorins Transport and Release Nitric Oxide. J. Am. Chem. Soc. 2008; 130:1611–1618. [PubMed: 18189390]

75. Swails JM, Meng Y, Walker FA, Marti MA, Estrin DA, Roitberg AE. pH Dependent Mechanism of Nitric Oxide Release in Nitrophorins 2 and 4. J. Phys. Chem. B. 2009; 113:1192–1201. [PubMed: 19159340]

76. Di Russo NV, Estrin DA, Marti MA, Roitberg AE. pH-Dependent Conformational Changes in Proteins and their Effect on Experimental pK_as: The Case of Nitrophorin 4. PLoS Comput. Biol. 2012; 8(11):e1002761. [PubMed: 23133364]

77. Berry RE, Shokhirev MN, Ho AYW, Yang F, Shokhireva TK, Zhang H, Weichsel A, Montfort WR, Walker FA. Effect of Mutation of Carboxyl Side-Chain Amino Acids Near the Heme on the Midpoint Potentials and Ligand Binding Constants of Nitrophorin 2 and Its NO, Histamine, and Imidazole Complexes. J. Am. Chem. Soc. 2009; 131:2313–2327. [PubMed: 19175316]

78. Hodsdon M, Cistola DP. Ligand Binding Alters the Backbone Mobility of Intestinal Fatty Acid-Binding Protein as Monitored by ^{15}N NMR Relaxation and ^{1}H Exchange. Biochemistry. 1997; 36:2278–2290. [PubMed: 9047330]

79. Qin BY, Creamer LK, Baker EN, Jameson GB. 12-Bromododecanoic Acid Binds inside the Calyx of Bovine β-Lactoglobulin. FEBS Lett. 1998; 438:272–278. [PubMed: 9827560]

80. Narayn M, Berliner LJ. Fatty Acids and Retinoids Bind Independently and Simultaneously to β-Lactoglobulin. Biochemistry. 1997; 36:1905–1911.

81. Dufour E, Marden MC, Haertlé T. β-Lactoglobulin Binds Retinol and Protoporphyrin IX at Two Different Binding Sites. FEBS Lett. 1990; 277:223–226. [PubMed: 2269359]

82. Brownlow S, Morais Cabral JH, Cooper R, Flower DR, Yewdall SJ, Polikarpov I, North ACT, Sawyer L. Bovine β-Lactoglobulin at 1.8 Å Resolution---Still an Enigmatic Lipocalin. Structure. 1997; 5:481–495. [PubMed: 9115437]

83. Kuwata K, Hoshino M, Forge V, Era S, Batt CA, Goto Y. Solution Structure and Dynamics of Bovine β-Lactoglobulin. Prot. Sci. 1999; 8:2541–2545.

84. Uhrinova S, Smith MH, Jameson GB, Uhrin D, Sawyer L, Barlow PN. Structural Changes Accompanying pH-Induced Dissociation of the β-Lactoglobulin Dimer. Biochemistry. 2000; 39:3565–3574. [PubMed: 10736155]

85. Ragona L, Catalano M, Luppi M, Cicero D, Elisea T, Foote J, Fogolari F, Zetta L, Molinari H. NMR Dynamic Studies Suggest that Allosteric Activation Regulates Ligand Binding in Chicken Liver Bile Acid-binding Protein. J. Biol. Chem. 2006; 281:9697–9709. [PubMed: 16439356]

86. Mills JL, Liu G, Skerra A, Szyperski T. NMR Structure and Dynamics of the Engineered Fluorescein-Binding Lipocalin, FluA Reveal Rigidification of β-Barrel and Variable Loops upon Enthalpy-Driven Ligand Binding. Biochemistry. 2009; 48:7411–7419. [PubMed: 19603796]

87. Muthu D, Berry RE, Yang F, Zhang H, Walker FA. Comparative NMR Studies of the Dynamics of High-Spin Nitrophorins 2 and 4 as a Function of pH, to be submitted.
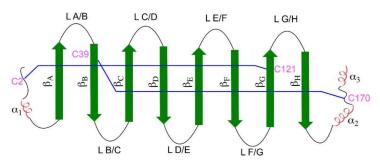
Figure 1.
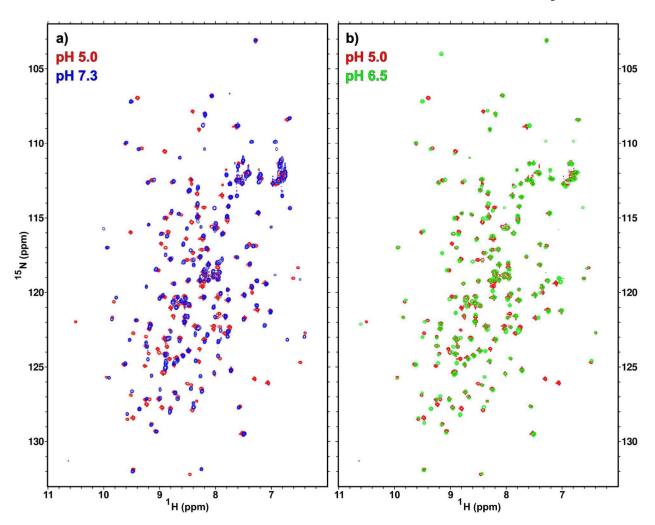Structure of NP2 and pattern of connections of disulfide bonds.

Figure 2.
a) Comparison of pH 5.0 (red) and 7.3 (blue) ^{1}H{^{15}N} HSQC plots for NP2-NO at 30 °C at 600 MHz ^{1}H frequency. b) Comparison of pH 5.0 (red) and 6.5 (green) HSQC plots for NP2-NO at 30 °C at 600 MHz ^{1}H frequency. Note the much greater similarity of the chemical shifts of most residues at the two pH values than seen in a).

Figure 3.
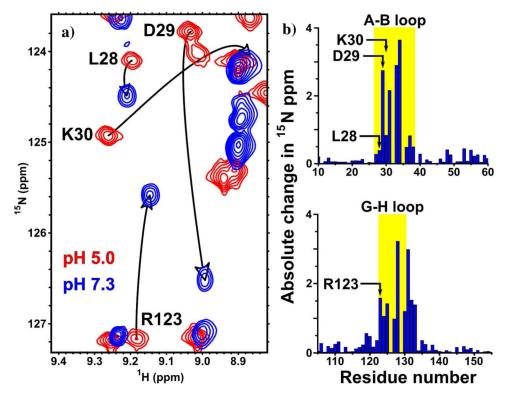**a)** Closeup of a comparison of the pH 5.0 and 7.3 HSQC plots for NP2-NO at 30 °C, recorded at 600 MHz, showing the dramatic change in the chemical shifts of several residues. **b)** Absolute change in ^{15}N chemical shift between these two pH values for the most-shifted residues (those of the A-B and G-H loops).
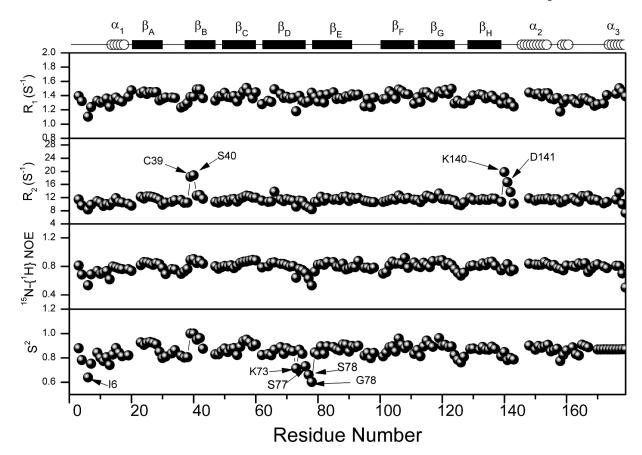
Figure 4.
[15]N relaxation data and calculated modelfree order parameter (S^2) of the native N-terminus NP2-NO complex measured at pH 5.0. The modelfree order parameters were obtained by fitting the raw data to the extended Lipari-Szabo modelfree formalism using *FASTModelfree* as described in the Materials and Methods. Errors are not shown for clarity. The location of β-sheets and helices are shown above the plot. A total of 29 non-proline residues could not be included in the calculation either because of overlap (27 residues) or not being assigned (2 residues).
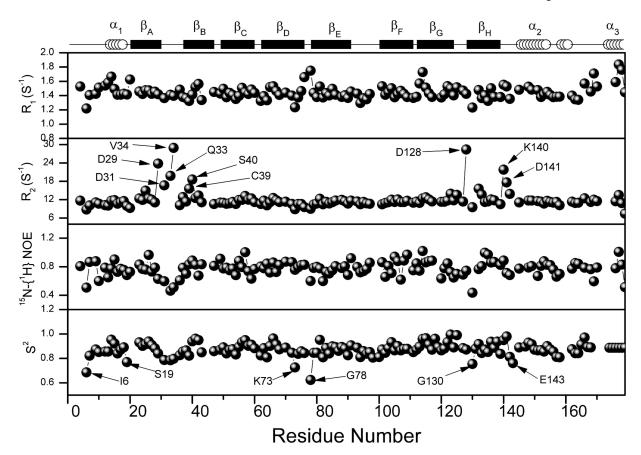
Figure 5.
[15]N relaxation data and calculated modelfree order parameter (S^2) of the native N-terminus NP2-NO complex measured at pH 7.3. The modelfree order parameters were obtained by fitting the raw data to the extended Lipari-Szabo modelfree formalism using FAST-Modelfree as described in the Materials and Methods. Errors are not shown for clarity. The location of β-sheets and helices are shown above the plot. A total of 30 non-proline residues could not be included in the calculation for various reasons such as signal overlap (15 residues), very weak signal intensity (7 residues) and not being assigned (8 residues).
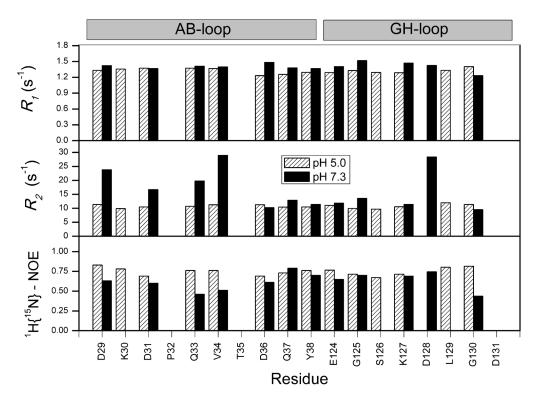
Figure 6.
Comparison of the modelfree data for R_1, R_2 and $^1H\{^{15}N\}$ NOE as a function of pH for the A-B and G-H loops, showing that R_1 is not affected, while R_2 and $^1H\{^{15}N\}$ NOE are significantly affected by the change in pH. This behavior of the R_2 values is consistent with the fact that the motions of the A-B loop in particular are on a much slower timescale than pico- to nanoseconds which are probed by the modelfree experiments.
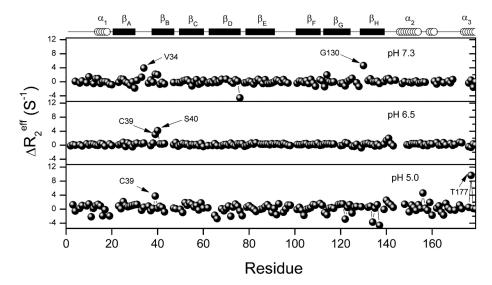
Figure 7.
Per residue plot of $\Delta R_2^{eff}(\nu_{CPMG})$ for the native N-terminus NP2-NO complex, showing motions in the micro- to millisecond timescale, at three different pH values (5.0, 6.5 and 7.3).

Table 1

Statistics of backbone dynamics of the NP2-NO complex at different pH values.

	pH 5.0	pH 6.5	pH 7.3
Relaxation Parameters			
R_1 (s^{-1}) av.	1.36 ± 0.07	1.41 ± 0.08	1.45 ± 0.10
$R2$ (s^{-1}) av.	11.44 ± 1.56	11.44 ± 2.9	12.00 ± 2.87
^{15}N{^{1}H} NOE av.	0.79 ± 0.07	0.78 ± 0.07	0.78 ± 0.10
Lipari-Szabo Model Parameters			
τ_m (ns)	8.61*	8.36*	8.41*
D_{ratio} ($D_{/\!/}D_\perp$)	1.09*	1.11*	0.95*
S^2 av.	0.854 ± 0.068	0.854 ± 0.076	0.874 ± 0.062
Number of residues			
Model 1 (S^2)	127	118	109
Model 2 (S^2, τ_e)	9	3	17
Model 3 (S^2, R_{ex})	4	12	8
Model 4 (S^2, τ_e, R_{ex})	0	1	7
Model 5 (S^2, S_f^2, τ_e)	5	10	3
No model assigned	1	2	1
Pro/overlapped peaks	33	33	34
Model 3 Specific residues	F66, K140, D141, A142	Q10, Q33, C39, F66, E110, D131, Y133, Q139, K140, D141, E143, C170	T25, Q37, C39, D128, D131, L132, Y133, K140
Relaxation Dispersion Parameters			
High $\Delta R_2^{eff}(\nu_{CPMG})$	C39, K140, G156, T177	C39, S40	D29, V34, S77, S114

Modelfree definitions: S^2: generalized order parameter; S_f^2: order parameter for very fast motions; τ_m: correlation time for macromolecular tumbling; τ_e: correlation time for internal motions; R_{ex}: contributions of microsecond to millisecond exchange phenomena to transverse relaxation; $D_{/\!/}$, $D_\perp$: components of the axial diffusion tensor.

*These values are from FastModelfree calculations after final optimization.